



# Photoinduced free radical-releasing systems and their anticancer properties

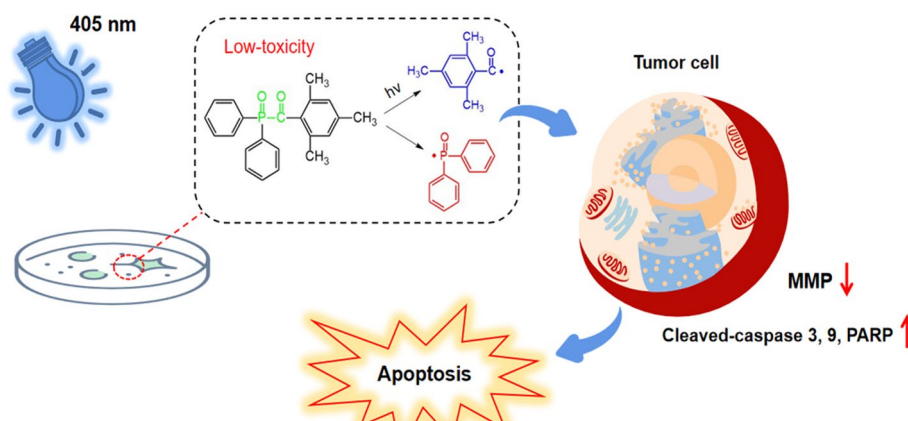
Jieyu Yan<sup>1</sup> · Haiwang Lai<sup>1</sup> · Boning Zeng<sup>1</sup> · Liqing Wang<sup>1</sup> · Feiyue Xing<sup>1,2</sup> · Pu Xiao<sup>3</sup>

Received: 24 March 2022 / Accepted: 11 April 2022 / Published online: 13 May 2022  
© The Author(s) 2022

## Abstract

Cancer has been a serious threat and impact on the health and life of human. Phototherapy is considered as a promising therapeutic method to replace the traditional treatment in clinic owing to its noninvasive nature and high efficiency. Photoinitiators have long been used in the field of photopolymerization; however, few studies have been carried out on their potential as anticancer agents under light irradiation. In this study, the effect of a photoinitiator, diphenyl (2, 4, 6-trimethylbenzoyl) phosphine oxide (TPO), on breast cancer is investigated and the related mechanism is elucidated. It is found that TPO has low dark toxicity and significant phototoxicity. TPO can inhibit cell growth and development and promote cell apoptosis through a mitochondrial pathway under light irradiation. Further studies show that cell apoptosis is induced by free radicals produced from the photolysis of TPO to activate JNK phosphorylation. Overall, we identify the antitumor effects of TPO in vitro for the first time, and provides a proof of concept for its application as a novel photolabile therapeutic drug.

## Graphical abstract



✉ Haiwang Lai  
555laihaiwang@163.com

✉ Feiyue Xing  
tfyxing@jnu.edu.cn

✉ Pu Xiao  
pu.xiao@anu.edu.au

<sup>1</sup> Department of Immunobiology, College of Life Science and Technology, Jinan University, #601 Huangpu West Avenue, Guangzhou 510632, China

<sup>2</sup> MOE Key Laboratory of Tumor Molecular Biology, Jinan University, Guangzhou 510632, China

<sup>3</sup> Research School of Chemistry, The Australian National University, Canberra, ACT 2601, Australia

## 1 Introduction

Malignant tumors have high morbidity and mortality, which cause millions of deaths annually. [1–3] With the development in fundamental knowledge of cancer biology, diagnosis, and treatment, the overall mortality rate of some common tumors has declined. At present, the commonly used clinical treatment methods include surgery, radiotherapy, chemotherapy, and hormone therapy [4]. However, all of these treatments have drawbacks or limitations, such as disturbing side effects, high treatment fees, and drug resistance

[5–8]. Within this context, non-invasive and non-destructive treatments have become increasingly attractive, attributing to the advantages including avoiding the unsightly scars and infection risks associated with surgery, reduced pain and discomfort, shorter recovery time, and more acceptable cost.

Phototherapy of tumors is minimal invasiveness with low side effects, principally containing photodynamic therapy (PDT) and photothermal therapy (PTT), offering new possibilities in cancer treatment [9–13]. PDT employs photosensitizers (PSs) to activate oxygen molecules into reactive oxygen species, such as singlet oxygen and superoxide anions, to kill cancer cells and destroy malignant tumor [14–16]. Therefore, the killing effect of PDT depends largely on oxygen concentration. Meanwhile, the hypoxic environment in tumor greatly reduces the efficacy of PDT [17, 18]. PTT, on the other hand, converts light energy into heat energy via photothermal transducing agents (PTAs) to heat the local areas and ablate tumors [19, 20]. Compared to PDT, PTT is not restricted by oxygen and only requires a suitable light source and efficient PTAs. Intriguingly, both Xia's group and Zhang's group took advantage of the photo-thermal effect of gold nanocages in combination with a thermal initiator 2,2'-azobis[2-(2-imidazoline-2-yl) propane] dihydrochloride (AIPH) to generate toxic alkyl radicals [21, 22]. These free radicals react directly with cellular components or oxygen to produce harmful free radicals. However, PTT or the combination with thermal initiators usually begins when the temperature reaches above 44 °C, which has problems, such as photothermal instability and poor photothermal conversion efficiency [23]. Besides, the actual temperature fluctuates greatly and is hard to control, which usually results in low therapeutic efficacy or overheating damage [24–26].

Photoinitiators (PIs) are widely used in fields, such as photocuring, 3D printing, and dental materials. PIs are well-developed, diverse, and inexpensive. According to the types of active species produced, PIs can be distinguished as free-radical and cationic PIs. Free-radical PIs can be further divided into cleavage type PIs (i.e., type I PIs) and hydrogen abstraction type PIs (i.e., type II PIs) [27–29]. Under the irradiation stimulation, type I PIs can directly photolyze into reactive radicals. Also, several researchers have employed radicals generated from PIs to eradicate cancer cells [30]. However, the mechanism for PIs to kill cancer cells remains unclear.

In this work, breast cancer (BC) cells were selected to explore the potential of PIs as anticancer agents under light irradiation. The cytotoxicity, phototoxicity, and other properties of three different type I PIs were compared. The investigated PIs include diphenyl (2,4,6-trimethyl benzoyl) phosphine oxide (TPO), 2-(4-Methoxystyryl)-4,6-bis(trichloromethyl)-1,3,5-triazine (triazine) and 2,4,6-trimethyl-benzoyl di-phenyl phosphinate (TPOL) (the structures are shown in Fig. 1). It is found that TPO is

the most promising PI due to its low dark cytotoxicity and significant phototoxicity under light exposure. The effect of TPO on the growth, migration, and death of breast cancer cells with or without irradiation and the mechanism of the TPO-mediated cancer cell death were further investigated. Our results provide a proof-of-concept basis for the application of PIs as potential new photosensitive anticancer drugs.

## 2 Materials and methods

### 2.1 Materials

Diphenyl (2,4,6-trimethyl benzoyl) phosphine oxide (TPO), 2,4,6-trimethyl-benzoyl di-phenyl phosphinate (TPOL) and 2-(4-methoxystyryl)-4,6-bis(trichloromethyl)-1,3,5-triazine (triazine) were provided from Tianjin Jiuri Co. (China). Methanol and diammonium 2,2'-azino-bis(3-ethylbenzothiazoline-6-sulfonate) (ABTS) were obtained from Guangdong Reagent Chemical Co. (China). *N*-acetyl cysteine (NAC), 2',7'-dichlorofluorescent yellow diacetate (DCFH-DA) and crystal violet (CV) were acquired from Sigma Chemical Co. (USA). Fetal bovine serum (FBS) was acquired from Gibco (USA). 3-(4,5-Dimethylthiazol-2-yl)-2,5-diphenyltetrazolium bromide (MTT), ethylene diaminetetraacetic acid (EDTA), Roswell Park Memorial Institute-1640 medium (RPMI-1640), Dulbecco's modified Eagle's medium (DMEM), Hoechst 33342, Annexin V/propidium iodide (PPI) kit and Calcein AM/PPI kit were purchased from Keygen BioTECH (China). Common antibodies associated with apoptosis, such as the Caspase family and JNK-related proteins, were all purchased from Cell Signaling Technology Co. (USA).

### 2.2 Methods

#### 2.2.1 Cell line and cultivation

Breast cancer cell line from human (MCF-7 cells) and mouse (4T1 cells) were acquired from the Cell Bank of Shanghai Institute of Cell Biology. MCF-7 and 4T1 cells were grown in DMEM or RPMI 1640 medium containing 10% (v/v) FBS and 100 µg/ml penicillin, respectively. The cells were provided with a high humidity atmosphere at a temperature of 37 °C and 5% CO<sub>2</sub>. When it reaches 80% confluence, cells were isolated by 0.25% trypsin supplemented with 0.01% EDTA.

#### 2.2.2 Cell viability analysis

The MTT assay was used to examine the influence of TPO on the viability of MCF-7 and 4T1 cells. Cells were seeded at a density of  $6 \times 10^3$  cells each well in 96-well plates and

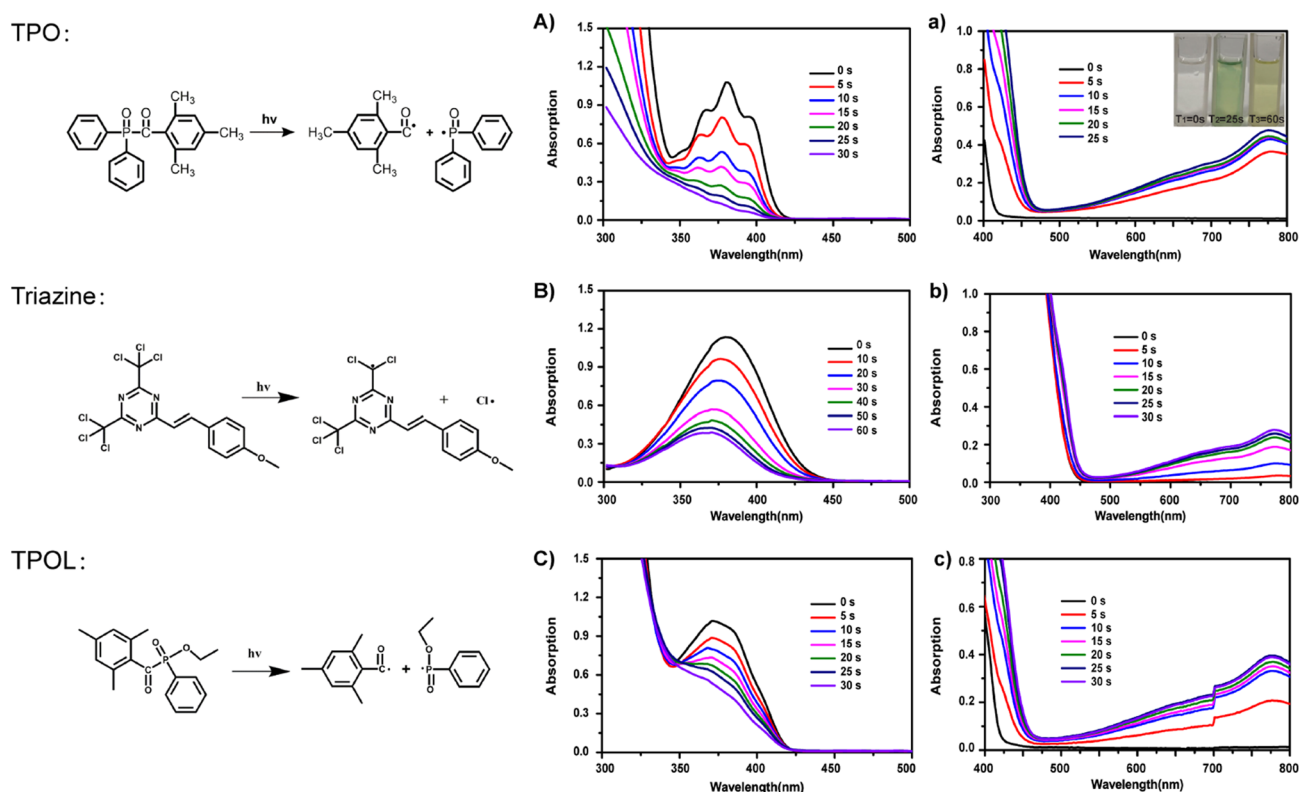


**Fig. 1** Investigation of free radical generating efficiencies of PIs. **A–C** UV/Vis spectra of **A** TPO (1 mM), **B** triazine (30 μM) and **C** TPOL (5 mM) irradiated with diverse time through LED@405 nm

(1 mM), **b** triazine (30 μM) and **c** TPOL (5 mM) with ABTS (3 mM) irradiated with different time through LED@405 nm

incubated overnight. TPO (5, 10, 20, 40 and 80 μM) was then applied to the cells and cultured in two kinds of environment [dark for up to 24 h or exposed to LED@405 nm for different irradiation times (0, 1, 5, 10, and 15 min)]. After adding MTT (0.5 mg/mL) and co-incubation with cells for 4 h, the liquid was aspirated, then DMSO was added to dissolve the purple formazan formed in the plate. Finally, using a microplate reader to measure the absorbance of different wells at 490 nm. Cell viability was calculated with formula:  $OD(\text{sample})/OD(\text{control}) \times 100\%$ .

### 2.2.3 Live/dead staining

Cells were seeded in 48-well plates with  $2 \times 10^4$  4T1 or MCF-7 cells per well. After cultivation of 24 h, the cells were washed with PBS and incubated with 200 μL of TPO-dissolved medium for 4 h (the concentration of TPO was 0, 5, and 20 μM). Following that, cells were subjected to LED@405 nm for 15 min. A working solution of 10 μM Calcein AM and 10 μM PPI in PBS was prepared and incubated together for 30–45 min. The staining solution was aspirated to terminate the incubation and the fluorescently labeled cells were checked by an inverted microscope.

### 2.2.4 Cell migration assay

Migration assays were carried out with cell chamber (Falcon, USA) in accordance with the manufacturer's protocol. After starvation for 12 h, the MCF-7 cells ( $6 \times 10^4$  cells each well) and 4T1 cells ( $1 \times 10^5$  cells each well) mixed with 200 μL medium without serum were delivered to the upper compartment of the transwell, while the lower compartment contained 800 μL of RPMI 1640/DMEM with 20% FBS. Methanol was used to fix cells that migrated to the lower compartment for 30 min, which were then stained with 0.1% crystal violet for 15 min at ambient temperature. Unmigrated parts were eliminated with a cotton swab. Finally, the migrated cells were observed and counted with an optical microscope (magnification  $\times 40$ ).

### 2.2.5 Extracellular free-radical generation

The determination method of ABTS was consistent with the previously reported method. The free radicals were measured by the reaction between TPO/TPOL/triazine solution and ABTS solution in DMF. The mixture was exposed to LED@405 nm for 5, 10, 15, 20, and 25 s. The absorbances

of the mixture within range of 400–800 nm were then recorded.

### 2.2.6 Intracellular free-radical detection

Using Hoechst 33342 and DCFH-DA fluorescent probes, the production of free radicals in cells was assessed. In a 24-well plate, MCF-7 and 4T1 cells were seeded with a density of  $2 \times 10^4$  cells per well and incubated overnight. Then, the cells were exposed to the diverse concentrations of TPO (0, 5, and 20  $\mu\text{M}$ ) for 4 h and irradiated by LED@405 nm for 15 min. Following TPO treatment, the culture medium was replaced with PBS containing DCFH-DA (10  $\mu\text{M}$ ) and Hoechst 33342 (5  $\mu\text{g}/\text{ml}$ ) and cultivated about 20 min. Fluorescence images were captured as soon as possible with a fluorescence microscope at 488 nm (magnification 40 $\times$ ).

### 2.2.7 Annexin V/propidium iodide (PPI) staining

The Annexin V/PPI apoptosis detection Kit (KeyGEN, China) was used to measure cell apoptosis according to the kit's protocol. 4T1 cells ( $1 \times 10^5$  cells each well) and MCF-7 cells ( $1.5 \times 10^5$  cells each well) were incubated in a six-well plate and then separated into light and dark groups. Following that, various TPO dosages were given. The light-groups were irradiated for 15 min by LED@405 nm after 4 h of growth. The cells were isolated and stained with 5  $\mu\text{M}$  of Annexin V and PPI. Finally, a flow cytometer was used to examine the samples.

### 2.2.8 Analysis of the mitochondrial membrane potential (MMP)

JC-1 was a well-established probe to the determine MMP. As required, 4T1 cells ( $1 \times 10^5$  cells per well) and MCF-7 cells ( $1.5 \times 10^5$  cells per well) were cultured in a 6-well plate. After 24 h, the cells were treated with different doses of TPO for 4 h. The light group was then irradiated by LED@405 nm for 15 min. Cells in all wells were collected. Then, the JC-1 staining solution was added to each EP tube to make the final concentration of 2  $\mu\text{M}$  and incubated at 37  $^\circ\text{C}$  for 20 min. The cells were washed and resuspended with PBS and further examined by flow cytometry.

### 2.2.9 Western blot analysis

In 6-well plates were seeded MCF-7 cells ( $1.5 \times 10^5$  cells per well) for 24 h in. Following TPO treatment, western

blotting is performed as follows: the prepared lysate buffer (RIPA lysate buffer to protease inhibitor ratio of 100:1) was applied to the plate on ice for 15 min. Following lysis, the supernatant liquid was subjected to centrifugation at a speed of 13,000g for 10 min. The concentration of collected protein were measure with a Bicinchoninic acid (BCA) kit. After gel electrophoresis, the protein band from the gel were transferred to a polyvinylidene fluoride (PVDF) membrane. Subsequently, 5% nonfat milk was prepared and the band on the membrane was blocked. TBST was used to rinse away residual skim milk. Then, the primary antibody was diluted according to the instructions and incubated with the membrane for 10–12 h at 4  $^\circ\text{C}$  (the dilution ratio is 1:2000). TBST was used to rinse away residual primary antibody for several times. Next, the washed membrane was continuously incubated with a second HR-conjugated antibody. Finally, protein visualization was performed by ECL chemiluminescence kit (Beyotime, China) or dark room. The protein's gray value was calculated using Image J program. Internal control was  $\beta$ -actin (CST, China, 1:500).

### 2.2.10 Statistical analysis

All experiments were carried out for three times independently, and the results were displayed by mean standard deviation (SD). The differences in pairwise comparisons were analyzed using the *T* test. As for the comparisons among various groups, one-way analysis of variance (ANOVA) was performed. Statistical difference was defined as probability values of  $*p < 0.05$ ,  $**p < 0.01$  and  $***p < 0.001$  or  $\#p < 0.05$ ,  $\#\#p < 0.01$ . In addition,  $*p < 0.05$ ,  $**p < 0.01$  and  $***p < 0.001$  vs. control,  $\#p < 0.05$ ,  $\#\#p < 0.01$  vs. dark group.

## 3 Results and discussion

### 3.1 Efficiency of free radical generation and phototoxicity of TPO, triazine and TPOL

Most PIs absorb light in the ultraviolet region. It is well known that ultraviolet rays are harmful to the human body. Therefore, PIs which can be activated under visible light irradiation were chosen in current study and visible light emitting diodes (LEDs) were used as the light source because of the higher safety and much narrower spectral line of LEDs compared to Xenon lamps and mercury arc lamps [31–33]. To this end, three PIs, TPO, triazine and

TPOL were chosen as potential photoactive anticancer agents due to their excellent photoinitiating efficiency under visible light irradiation. Bisacylphosphane oxides (BAPO) has been reported to have many potential applications as a drug with extraordinary photopotential toxicity and anticancer properties [30]. However, it was shown that the BAPO had a significant cytotoxicity to normal human cells, while TPO and TPOL had low toxicity [34]. Meanwhile, it is demonstrated that triazine was a highly efficient type I PI that initiated free radical photopolymerization under visible LED by generating chlorine radicals  $\text{Cl}\cdot$  and chloro-carbon radicals  $\text{Cl-C}\cdot$  [34, 35].

The decomposition performance of TPO, triazine and TPOL were first investigated via measuring their absorbance under irradiation of LED@405 nm. The characteristic peaks of the TPO, triazine and TPOL were all rapidly decreased upon exposure of LED@405 nm, as shown in Fig. 1A–C, indicating the decomposition of PIs. Furthermore, ABTS was used to indicate the generation of radical species. ABTS itself is colorless, while the solution of  $\text{ABTS}^{+\bullet}$  formed after the reaction of ABTS and PIs radicals is green with characteristic absorption peak in the range of 600–900 nm. The absorption of  $\text{ABTS}^{+\bullet}$  rises with time, suggesting that all PIs consistently created free radicals when exposed to LED@405 nm irradiation (Fig. 1a–c). In comparison, no change of UV spectrum could be observed from the ABTS alone or ABTS with PIs in dark (Fig. S1), implying that the free radicals were created by photo-induced breakdown of PIs.

An ideal PI to be used as anticancer agents requires low dark toxicity and strong phototoxicity. Therefore, the MTT assay was chosen to detect the photo-dark cytotoxicity of TPOL, TPO and triazine. As shown in Fig. 2A, triazine is highly toxic in dark compared to the control.

The cell viability was only  $47.66 \pm 1.31\%$  when the concentration was  $5 \mu\text{M}$ . However, the dark cytotoxicity of TPO and TPOL only manifested when the concentration was above  $40 \mu\text{M}$  ( $p < 0.05$ ). Upon light irradiation, TPO had a higher toxicity than TPOL (Fig. 2B, C). Overall, these chosen PIs can indeed generate free radicals by photodissociation; however, only TPO had weak dark toxicity and strong phototoxicity. Thus, TPO was selected as the candidate anticancer agent for subsequent research.

### 3.2 TPO inhibits the proliferation and migration of breast cancer cells

Increasing evidences have shown that low levels of free radicals promote cell proliferation, whereas excessive accumulation of free radicals can injure cell components, for example the proteins, lipids and nucleic acids, ultimately leading to cell death [36]. The effects of TPO on cell growth and development were subsequently investigated. We evaluated the cytotoxicity of TPO at different concentrations with different irradiation time through MTT assay. As depicted in Fig. 3A, the concentration of TPO had a relatively moderate influence on cell viability in the dark group, and only when the concentration was larger than  $40 \mu\text{M}$  did the cell viability differ significantly from the control group ( $p < 0.05$ ). The growth of 4T1 cells in the light group was considerably reduced when TPO concentration increased ( $p < 0.05$ ). Furthermore, prolonged irradiation period significantly hindered cell development. The  $\text{IC}_{50}$  values of TPO exposed to LED@405 nm for 5, 10, and 15 min were 31.78, 27.5 and  $22.63 \mu\text{M}$ , respectively. Similarly, the inhibitory effect of TPO on MCF-7 cell viability was still contingent on dose

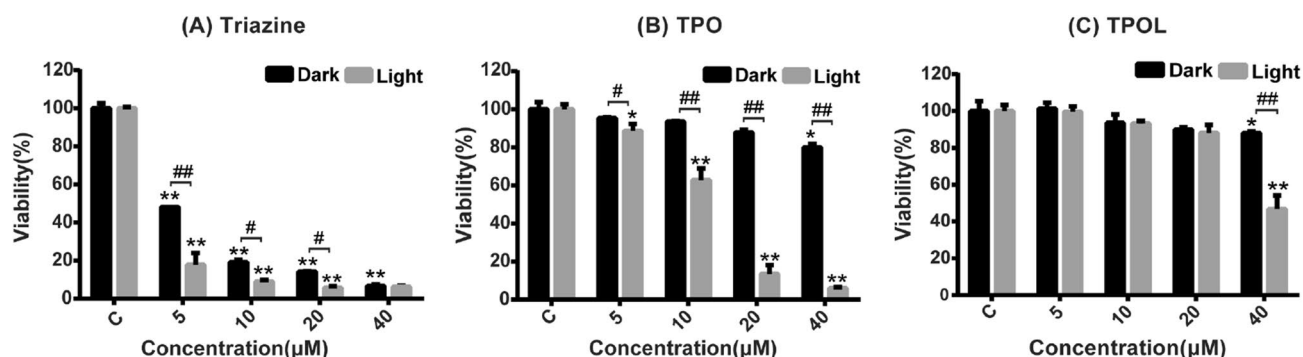


**Figure 2.** Phototoxicity of the TPO, triazine and TPOL. 4T1 cells were exposed to **A** triazine, **B** TPO and **C** TPOL. They were utilized for diverse concentrations (0, 5, 10, 20, and  $40 \mu\text{M}$ ) with or without

the irradiation (LED@405 nm, Distance=30 cm, Time=15 min). Results are described by the means  $\pm$  SD of triplicate experiments. # $p < 0.05$ , ## $p < 0.01$  vs. dark group, \* $p < 0.05$ , \*\* $p < 0.01$  vs. control

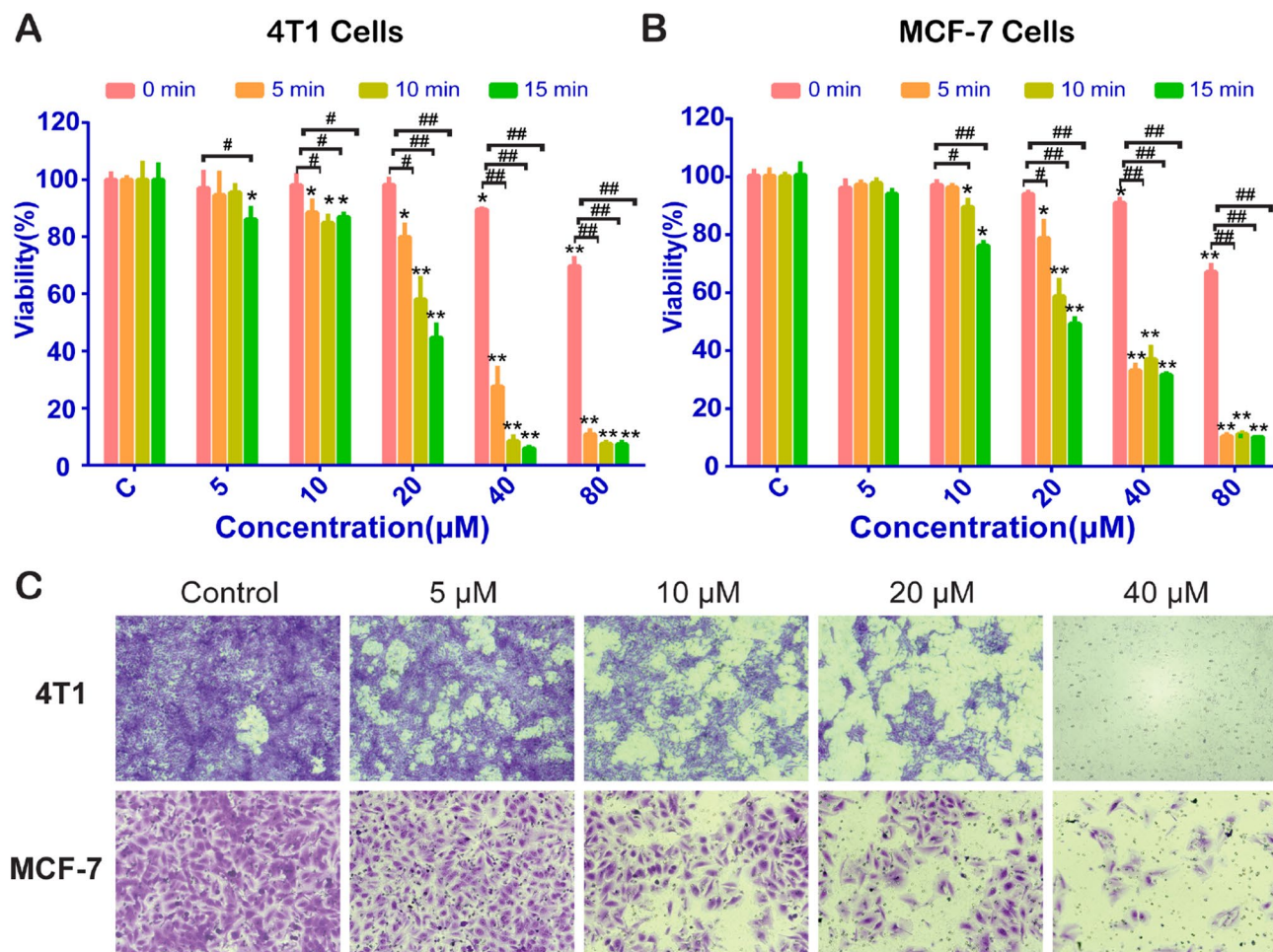


**Fig. 3** TPO suppresses the proliferation and migration of breast cancer cells and promotes cell death after irradiation. **A** The 4T1 cells and **B** MCF-7 cells were treated with TPO (0, 5, 10, 20, 40 and 80 μM) with irradiation (LED@405 nm, Distance=30 cm) for various time (0, 5, 10 and 15 min) to evaluate cytotoxicity by means of

MTT assay. **C** Transwell migration assays. Microscopic images of MCF-7 and 4T1 cells migrating through the transwell in the migration assay. (Magnification 200, Giemsa stain). Results are described by the means  $\pm$ SD of triplicate experiments. # $p < 0.05$ , ## $p < 0.01$  vs. dark group, \* $p < 0.05$ , \*\* $p < 0.01$  vs. control

and irradiation time (Fig. 3B). However, under the same conditions, 4T1 cells were more sensitive than MCF-7 cells.

Since the cell migration ability is of great significance in the formation and development of malignant tumors. Next, we performed transwell experiments to test whether TPO inhibited the migration of BC cells. As proven in Fig. 3C, the migration ability of 4T1 and MCF-7 cells progressively decreased with increasing TPO concentration. These data collectively indicated that TPO under irradiation of LED@405 nm obviously inhibited the proliferation and migration of BC cells dependent on dosage and irradiation time, showing promise to hinder further tumor development. However, reasons behind this phenomenon need to be further explored.

### 3.3 TPO induces apoptosis of breast cancer cells

To observe the cancer cell-killing effect of TPO more intuitively, MCF-7 and 4T1 cells were labeled with Calcein AM and PPI, with green fluorescence signifying viable cells and red fluorescence signifying dead cells. A fluorescent microscope was then used to collect the fluorescence images (Fig. 4A, B). It could be observed that almost all cells fluoresced green in the dark groups and the TPO-untreated while irradiated group, suggesting that TPO or 405 nm LED illumination alone is harmless to cells. As expected, upon irradiation (405 nm, 15 min), significant red fluorescence (dead cells) was observed, indicating the population of dead cells increases with increasing concentration of TPO (Fig. 4C, D).

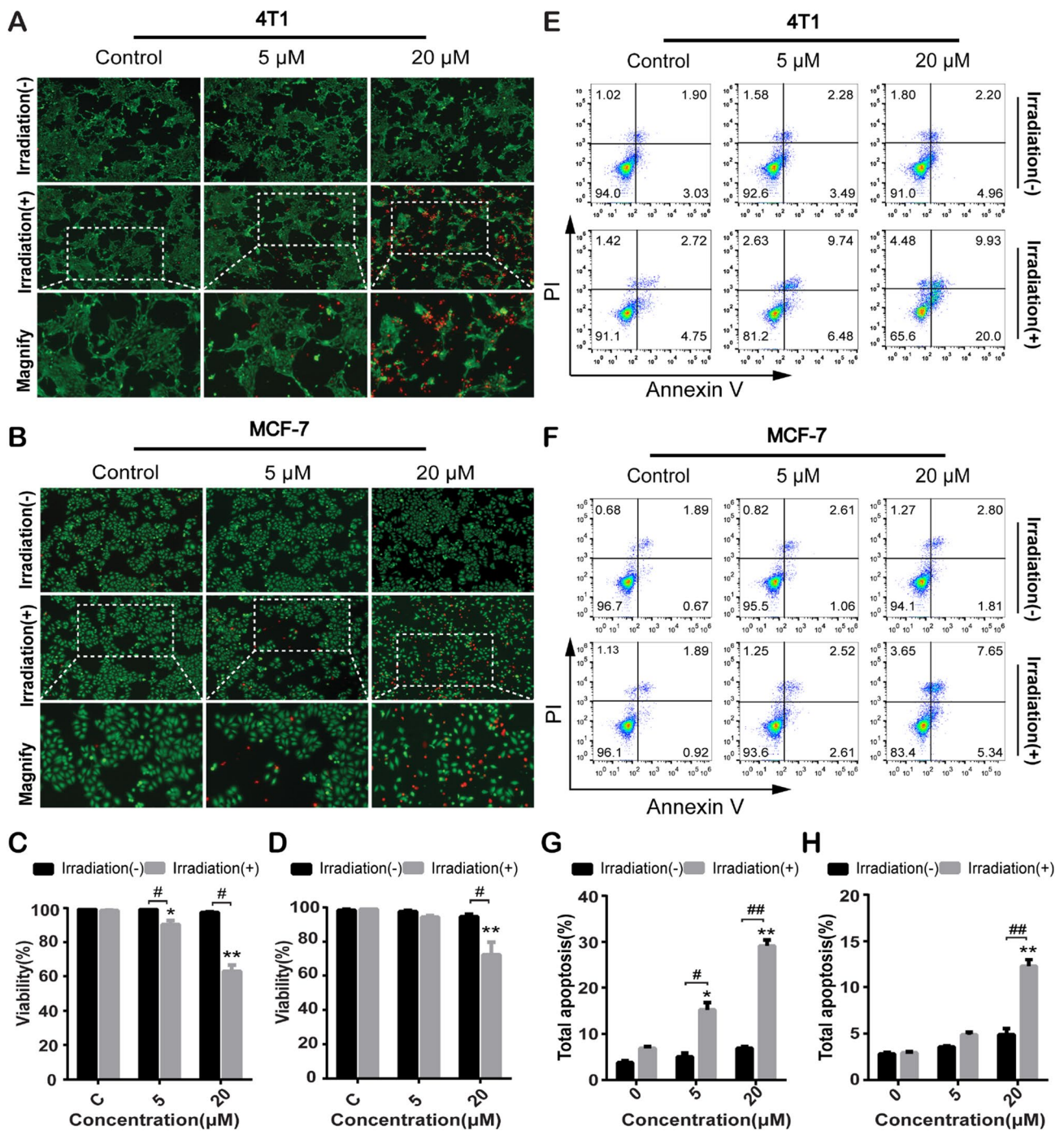


**Fig. 4** TPO induces apoptosis of breast cancer cells. Fluorescence images of **A** 4T1 cells and **B** MCF-7 cells co-stained by Calcein AM/PPI following TPO treatment. (0, 5, 20  $\mu$ M). Viable cells were presented in green and dead cells were presented in red, respectively (Magnification:  $\times 100$ ). **C** Statistical analysis of 4T1 cells. **D** Statistical analysis of MCF-7 cells. Apoptosis assay of **E** 4T1 and **F** MCF-7

cells using flow cytometry after staining with Annexin V/PPI. Cells were treated with 0, 5, 20  $\mu$ M of TPO with or without irradiation for 15 min. Scatter plots showing PPI (y-axis) vs. annexin V (x-axis). Percentage of the apoptotic **G** 4T1 cells and **H** MCF-7 cells. Results are described by the means  $\pm$  SD of triplicate experiments. #  $p < 0.05$ , ##  $p < 0.01$  vs. dark group, \*  $p < 0.05$ , \*\*  $p < 0.01$  vs. control

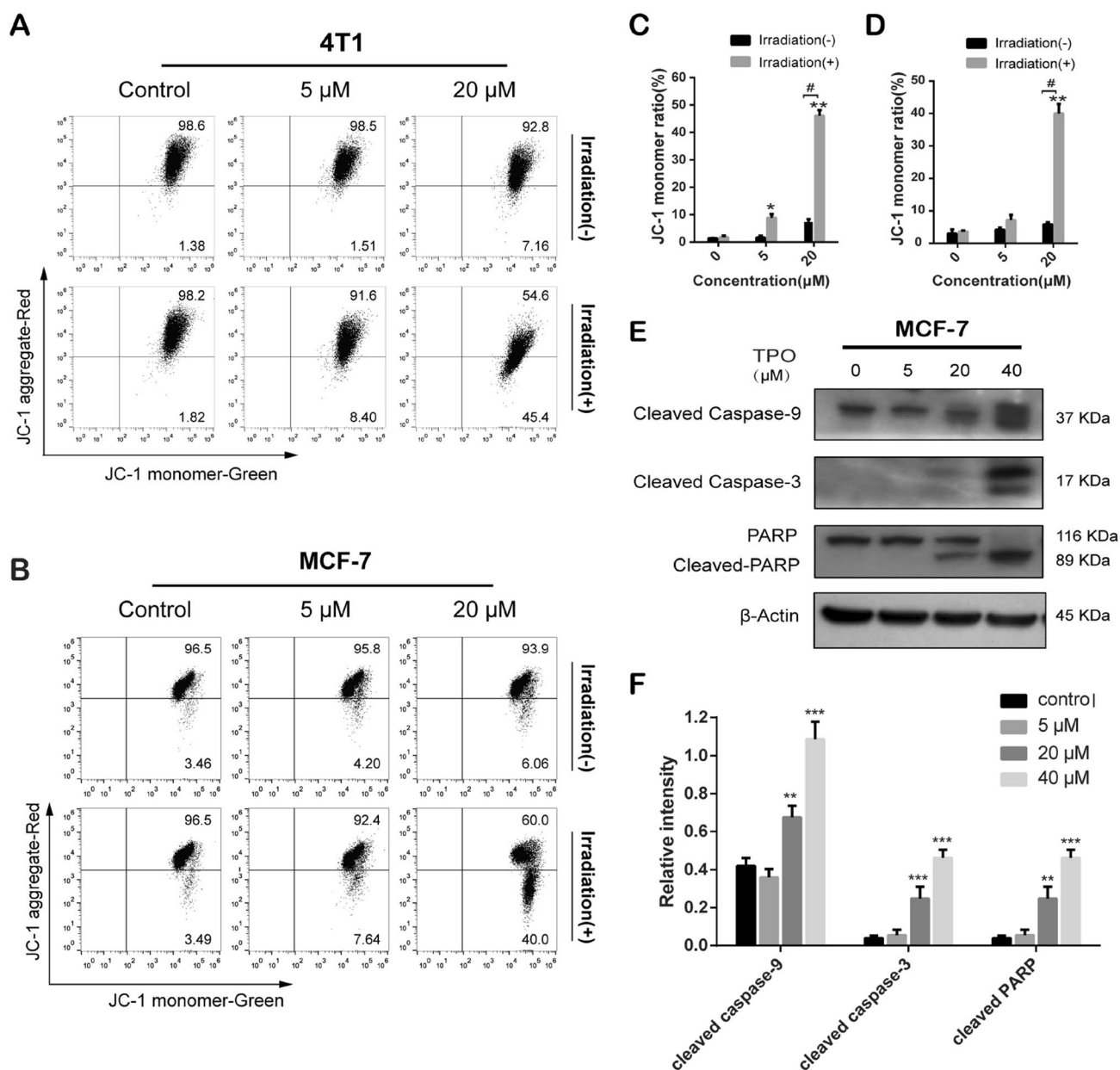


**Fig. 5** TPO induces apoptosis through the mitochondrial apoptotic pathway. Flow cytometry detection of MMP in **A** 4T1 and **B** MCF-7 cells induced by TPO using the JC-1 assay. **C** Statistical analysis of the proportion of JC-1 monomer in 4T1 cells. **D** Statistical analysis of the proportion JC-1 monomer in MCF-7 cells. **E** Western blot

analyses of apoptosis-associated proteins separated by SDS-PAGE. **F** Grayscale analysis of protein bands. Results are described by the means  $\pm$  SD of triplicate experiments. # $p < 0.05$ , ## $p < 0.01$  vs. dark group, \* $p < 0.05$ , \*\* $p < 0.01$  vs. control

Annexin V/PPI staining and flow cytometry testing were chosen to explore if TPO can promote apoptosis. More than 95% of the alive cells were observed in both the irradiated and non-irradiated control groups, as illustrated in Fig. 4E,F. Cells incubated with TPO in dark showed

negligible cytotoxicity, and cell viability remained above 90%. However, upon LED@405 nm irradiation, the cell apoptosis rate increased dramatically as TPO concentration increased. As shown in Fig. 4G, the apoptotic rates of 4T1 cells at 5  $\mu$ M ( $16.22 \pm 1.26\%$ ) and 20  $\mu$ M ( $29.93 \pm 1.08\%$ ) of TPO were significantly higher as



compared with the control group ( $7.53 \pm 0.67\%$ ,  $p < 0.05$ ). Likewise, the apoptotic rate of MCF-7 cells at the 0, 5, and 20  $\mu\text{M}$  were  $2.94 \pm 0.1\%$ ,  $5.13 \pm 0.23\%$  and  $12.99 \pm 0.61\%$  (Fig. 4H), respectively. All these data confirm that TPO has a cancer cell killing ability only upon light irradiation and TPO inhibits cancer cell proliferation via inducing cell apoptosis.

### 3.4 TPO induces apoptosis through the mitochondrial apoptotic pathway

Next, we employed the JC-1 probe to confirm mitochondrial participation in TPO-induced apoptosis. As shown in Fig. 5A,B, flow cytometry results showed that cells treated or untreated with TPO without irradiation were well-polarized. TPO treatment resulted in a great transition from red to green fluorescence in BC cells when exposed to LED@405 nm (Fig. 5C), demonstrating that TPO promoted mitochondrial depolarization. As illustrated in Fig. 5C, the ratio of 4T1 cells with high membrane potential decreased from 98.2 to 91.6% after exposed to 5  $\mu\text{M}$  TPO and even decreased to 54.6% in 20  $\mu\text{M}$  TPO treated group. Likewise, the loss of mitochondrial potential in MCF-7 cells caused by TPO also showed dose-dependent manner (Fig. 5D).

To further clarify whether TPO-induced apoptosis is mediated by an extrinsic or intrinsic pathway, we utilized western blotting to explore the expression of downstream apoptotic-associated proteins. As shown in Fig. 5E,F, the expression levels about cleaved caspase-3, -9 and PARP were dramatically elevated. Overall, these results confirmed that the involvement of the apoptotic pathway in cell mortality.

### 3.5 TPO activates the JNK pathway by inducing free radical generation

Free radicals act as an irreplaceable role in various biochemical functions. Alteration of intracellular free radical levels are closely related to tumorigenesis and is also considered a valuable strategy for the treatment of cancer [37, 38]. Based on the results above, it is verified that TPO can undergo photolysis to release free radicals after irradiation. We then used the DCFH-DA probe to examine the generation of free radicals in cancer cells with combined fluorescence microscopy and flow cytometry. As shown in Fig. 6A,B, the cells treated with the TPO and DCFH-DA in the dark did not show any formation of DCF. Upon irradiation, free radicals were released dramatically by TPO treatment, as indicated by the increase in green fluorescence signal. Furthermore, we applied NAC (free-radical scavenger) to validate the

elevation of free radicals. (Fig. 6C,D). It is found that NAC pretreatment can effectively reduce the free radicals induced by TPO.

Following that, we examined the effect of TPO on the JNK pathway. As present in Fig. 6E, JNK phosphorylation is enhanced with increasing TPO dose. However, the JNK inhibitor SP600125 successfully reversed JNK phosphorylation and prevented JNK pathway activation (Fig. 6F). The JNK pathway has been validated to be activated through a range of environmental stresses, such as oxidative stress. It is further found that the activation of JNK pathway can be effectively inhibited by NAC pretreatment (Fig. 6G). These results revealed that irradiated-TPO spark off the JNK pathway by generating radicals, which might immediately promote mitochondrial permeability to initiate apoptosis.

### 3.6 TPO induces apoptosis via the activation of free radical/JNK pathway

JNK signaling pathway, act as a key stress signal transduction pathway, is commonly activated in response to adverse environmental stimuli. Thus, it can determine the fate of the cells. Although increasing researches have indicated that JNK was pro-survival in some cell types, abnormal activation of JNK still plays an irreplaceable role in the mitochondria-dependent intrinsic apoptosis pathway and is considered to be an important driver of apoptosis [39, 40].

To explore whether TPO-induced apoptosis is related to the generation of free radicals and JNK activation, the related protein levels were detected by western blotting. The cells were intervened with either SP600125 or the free radical scavenger NAC. The results were displayed in Fig. 7. Compared to the TPO treatment, the presence of both SP600125 and NAC could reduce the expression of proteins to some extent, indicating that the both of them alleviated the cell apoptosis caused by light-irradiated TPO. These data imply that TPO-induced free radical/JNK pathway activation might strongly correlated in apoptosis induction. Using the JNK inhibitor SP600125 (Fig. 7C,D), it was demonstrated that TPO-induced apoptosis is associated with JNK activation. Moreover, free radicals can promote JNK pathway activation, whereas early intervention with NAC receded the phosphorylation of JNK (Fig. 7A,B). These data suggested that irradiated TPO releases free radicals that induce apoptosis through activating the free radical-dependent JNK pathway by activating caspase-9, caspase-3 and PARP (Fig. 8).

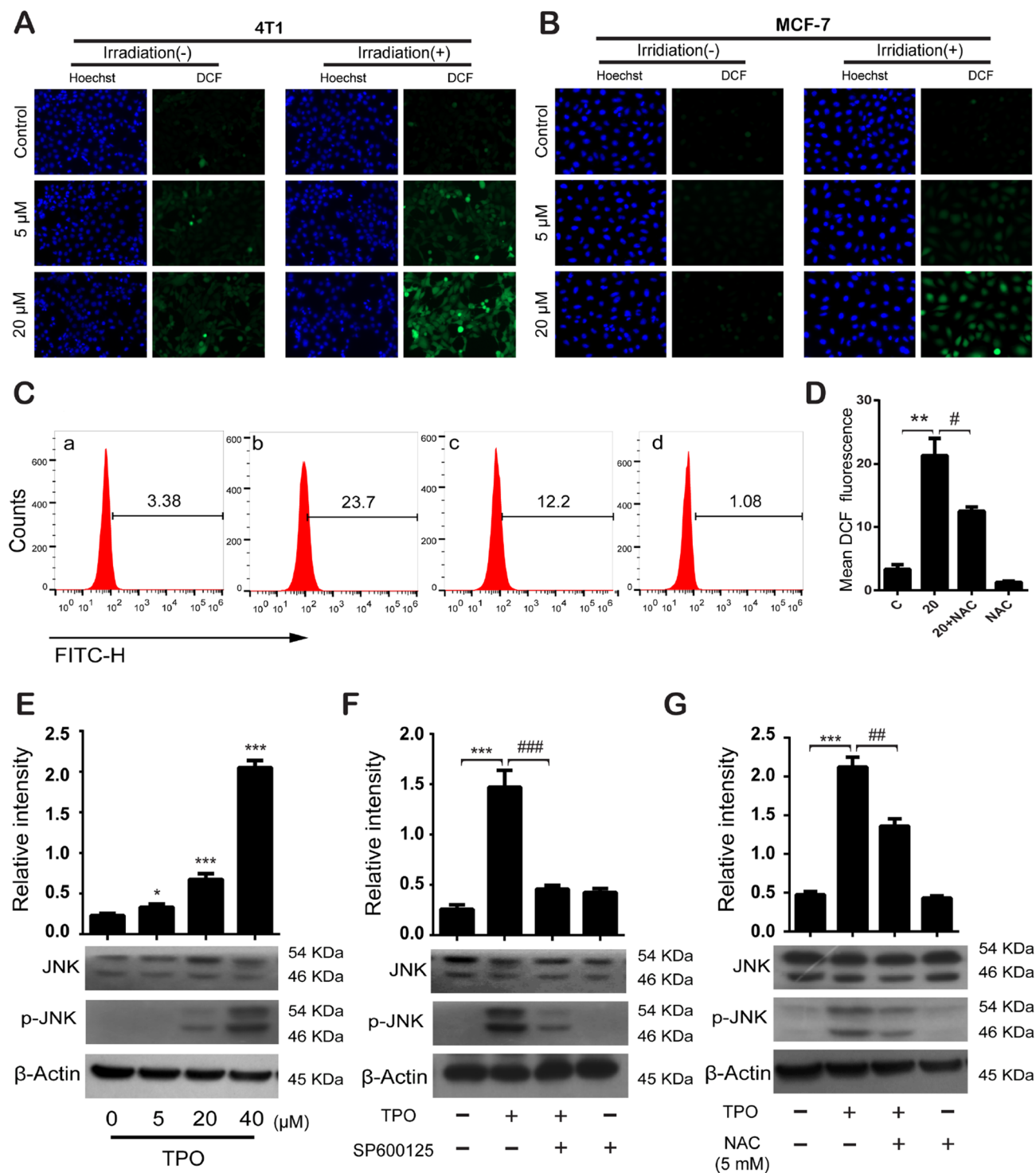


**Figure 6.** TPO activates the JNK pathway by inducing free radical generation. **A** The 4T1 and **B** MCF-7 cells were treated with TPO (0, 5, 20  $\mu\text{M}$ ) exposed to LED@405 nm for 15 min. Photographs were taken using a fluorescence microscope. (Magnification:  $\times 100$ ). **C** Flow cytometry analysis the generation of free radicals. MCF-7 cells were grown with **a** control, **b** 20  $\mu\text{M}$  TPO, **c** 20  $\mu\text{M}$  TPO+5 mM NAC, **d** 5 mM NAC and exposed to LED@405 nm for 15 min, respectively. And then incubated with DCFH-DA for 30 min at 37  $^{\circ}\text{C}$ .

**D** Statistical analysis of fluorescence intensity of DCF. **E** After being treated with various dosages of TPO for 4 h, cells were exposed to LED@405 nm for 15 min. Using western blotting to examine the expression level of p-JNK and JNK. **F**, **G** Cells were preincubated for 2 h with SP600125 (a JNK inhibitor, 25 M) or NAC (5 mM), TPO was added and incubated for 4 h, and exposed to LED@405 nm for 15 min. Levels of p-JNK and JNK were analyzed. Results are described by the means  $\pm$  SD.  $n = 3$ ,  $*p < 0.05$ ,  $**p < 0.01$

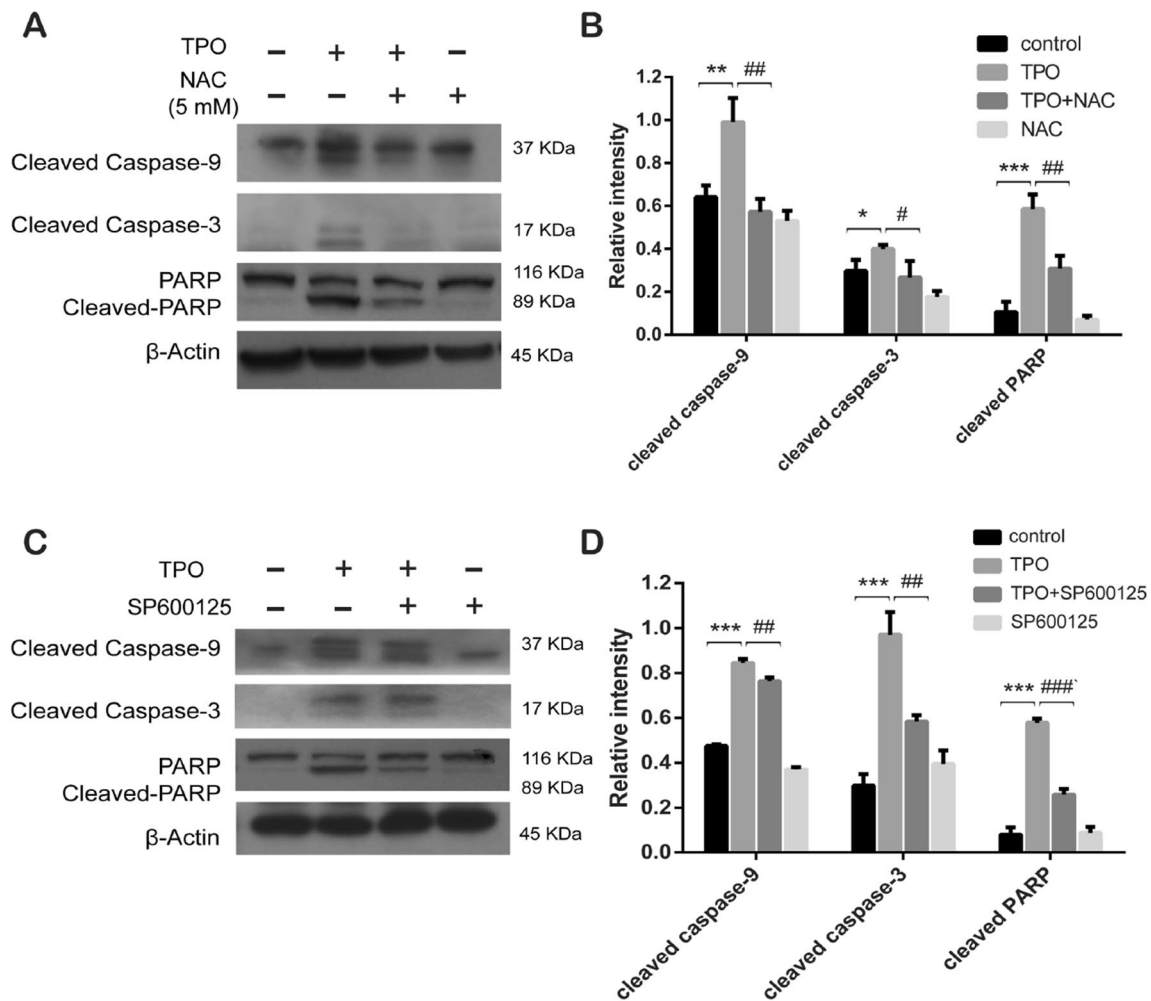


**Fig. 7** TPO induces apoptosis via the activation of free radical/JNK pathway. Cells were pretreated with SP600125 (25  $\mu$ M) or NAC (5 mM) for 2 h, then treated with TPO for 4 h and exposed to LED@405 nm for 15 min. **A, C** Detection of the apoptosis-associated

proteins by western blotting. **B, D** Grayscale analysis of protein bands. Results are described by the means  $\pm$  SD of triplicate experiments. ## $p$  < 0.01 and ### $p$  < 0.001 vs. TPO-treated group, \* $p$  < 0.05, \*\* $p$  < 0.01 and \*\*\* $p$  < 0.001 vs. control, # $p$  < 0.05

## 4 Conclusions

In summary, our research identifies the anti-tumor function of TPO on breast cancer cells in vitro for the first time. TPO has low dark toxicity and significant phototoxicity. When irradiated with light, TPO restrained the cell growth and migration of breast cancer cells, inducing cell death in a concentration- and irradiation time-dependent manner. This impact is associated with the free radicals generated

by photolysis. The mechanism may be that the generated free radicals break the redox balance in the cell, raise cell oxidative stress, activate the JNK signal pathway, initiate the mitochondria-dependent intrinsic apoptosis, and cause the activation of caspase-9, caspase-3 and PARP. This study broadens the application field of photoinitiators and provides a proof of concept for them as novel phototherapeutic drugs with anticancer potential. Moreover, diverse and well-investigated type II photoinitiators, either one-component or multi-component photoinitiators [41, 42], can also be used

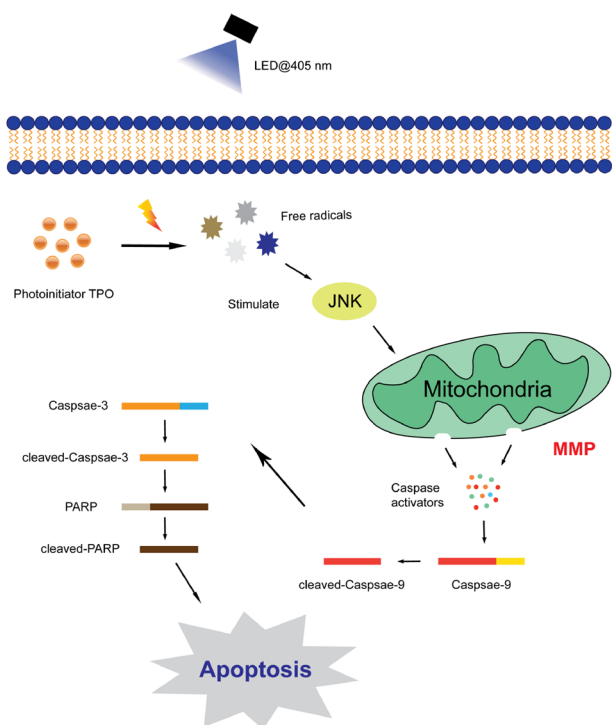


**Figure 8.** Schematic illustration of the roles of free radicals and JNK in irradiated-TPO induced mitochondria-dependent endogenous apoptosis

for phototherapeutic purpose, especially for those used in dentistry with proved biosafety.

**Acknowledgements** H.L. thanks the financial support by China Postdoctoral Science Foundation Grant (2019TQ0119).

**Funding** Open Access funding enabled and organized by CAUL and its Member Institutions.

## Declarations

**Conflict of interest** On behalf of all authors, the corresponding author states that there is no conflict of interest.

**Open Access** This article is licensed under a Creative Commons Attribution 4.0 International License, which permits use, sharing, adaptation, distribution and reproduction in any medium or format, as long as you give appropriate credit to the original author(s) and the source, provide a link to the Creative Commons licence, and indicate if changes were made. The images or other third party material in this article are included in the article's Creative Commons licence, unless indicated otherwise in a credit line to the material. If material is not included in the article's Creative Commons licence and your intended use is not permitted by statutory regulation or exceeds the permitted use, you will need to obtain permission directly from the copyright holder. To view a copy of this licence, visit <http://creativecommons.org/licenses/by/4.0/>.

## References

- Sung, H., Ferlay, J., Siegel, R. L., Laversanne, M., Soerjomataram, I., Jemal, A., & Bray, F. (2021). Global cancer statistics 2020: GLOBOCAN estimates of incidence and mortality worldwide for 36 cancers in 185 countries. *CA: A Cancer Journal for Clinicians*, 71(3), 209–249. <https://doi.org/10.3322/caac.21660>
- Siegel, R. L., Miller, K. D., Fuchs, H. E., & Jemal, A. (2021). Cancer Statistics, 2021. *CA: A Cancer Journal for Clinicians*, 71(1), 7–33. <https://doi.org/10.3322/caac.21654>
- Siegel, R. L., Miller, K. D., & Jemal, A. (2020). Cancer statistics, 2020. *CA: A Cancer Journal for Clinicians*, 70(1), 7–30. <https://doi.org/10.3322/caac.21590>
- Chen, X., Xu, D., Li, X., Zhang, J., Xu, W., Hou, J., et al. (2019). Latest overview of the cyclin-dependent kinases 4/6 inhibitors in breast cancer: The past, the present and the future. *Journal of Cancer*, 10(26), 6608–6617. <https://doi.org/10.7150/jca.33079>
- Chen, Y., Jungsuwadee, P., Vore, M., Butterfield, D. A., & St Clair, D. K. (2007). Collateral damage in cancer chemotherapy: Oxidative stress in nontargeted tissues. *Molecular Interventions*, 7(3), 147–156. <https://doi.org/10.1124/mi.7.3.6>
- Wu, J., & Waxman, D. J. (2018). Immunogenic chemotherapy: Dose and schedule dependence and combination with immunotherapy. *Cancer Letters*, 419, 210–221. <https://doi.org/10.1016/j.canlet.2018.01.050>
- Gottesman, M. M., Fojo, T., & Bates, S. E. (2002). Multidrug resistance in cancer: Role of ATP-dependent transporters. *Nature Reviews Cancer*, 2(1), 48–58. <https://doi.org/10.1038/nrc706>
- Bray, F. N., Simmons, B. J., Wolfson, A. H., & Nouri, K. (2016). Acute and chronic cutaneous reactions to ionizing radiation therapy. *Dermatology Therapy (Heidelb)*, 6(2), 185–206. <https://doi.org/10.1007/s13555-016-0120-y>
- Chilakamarthi, U., & Giribabu, L. (2017). Photodynamic therapy: Past, present and future. *Chemical Record*, 17(8), 775–802. <https://doi.org/10.1002/tcr.201600121>
- Greenwald, B. D. (2000). Photodynamic therapy for esophageal cancer. Update. *Chest Surgery Clinical North America*, 10(3), 625–637.
- Dai, X., Du, T., & Han, K. (2019). Engineering nanoparticles for optimized photodynamic therapy. *ACS Biomaterials Science and Engineering*, 5(12), 6342–6354. <https://doi.org/10.1021/acsbiomaterials.9b01251>
- Donohoe, C., Senge, M. O., Arnaut, L. G., & Gomes-da-Silva, L. C. (2019). Cell death in photodynamic therapy: From oxidative stress to anti-tumor immunity. *Biochimica et Biophysica Acta—Reviews on Cancer*, 1872(2), 188308. <https://doi.org/10.1016/j.bbcan.2019.07.003>
- Garg, A. D., Nowis, D., Golab, J., & Agostinis, P. (2010). Photodynamic therapy: Illuminating the road from cell death towards anti-tumour immunity. *Apoptosis*, 15(9), 1050–1071. <https://doi.org/10.1007/s10495-010-0479-7>
- Brackett, C. M., & Gollnick, S. O. (2011). Photodynamic therapy enhancement of anti-tumor immunity. *Photochemical and Photobiological Sciences*, 10(5), 649–652. <https://doi.org/10.1039/c0pp00354a>
- Naidoo, C., Kruger, C. A., & Abrahamse, H. (2018). Photodynamic therapy for metastatic melanoma treatment: A review. *Technology in Cancer Research and Treatment*, 17, 1533033818791795. <https://doi.org/10.1177/1533033818791795>
- Castano, A. P., Demidova, T. N., & Hamblin, M. R. (2005). Mechanisms in photodynamic therapy: Part two-cellular signaling, cell metabolism and modes of cell death. *Photodiagnosis*

- and Photodynamic Therapy, 2(1), 1–23. [https://doi.org/10.1016/S1572-1000\(05\)00030-X](https://doi.org/10.1016/S1572-1000(05)00030-X)
17. Fan, W., Huang, P., & Chen, X. (2016). Overcoming the Achilles' heel of photodynamic therapy. *Chemical Society Reviews*, 45(23), 6488–6519. <https://doi.org/10.1039/c6cs00616g>
  18. Li, X., Kwon, N., Guo, T., Liu, Z., & Yoon, J. (2018). Innovative strategies for hypoxic-tumor photodynamic therapy. *Angewandte Chemie (International ed. in English)*, 57(36), 11522–11531. <https://doi.org/10.1002/anie.201805138>
  19. Yu, J., Javier, D., Yaseen, M. A., Nitin, N., Richards-Kortum, R., Anvari, B., & Wong, M. S. (2010). Self-assembly synthesis, tumor cell targeting, and photothermal capabilities of antibody-coated indocyanine green nanocapsules. *Journal of the American Chemical Society*, 132(6), 1929–1938. <https://doi.org/10.1021/ja908139y>
  20. Jung, H. S., Verwilt, P., Sharma, A., Shin, J., Sessler, J. L., & Kim, J. S. (2018). Organic molecule-based photothermal agents: An expanding photothermal therapy universe. *Chemical Society Reviews*, 47(7), 2280–2297. <https://doi.org/10.1039/c7cs00522a>
  21. Shen, S., Zhu, C., Huo, D., Yang, M., Xue, J., & Xia, Y. (2017). A hybrid nanomaterial for the controlled generation of free radicals and oxidative destruction of hypoxic cancer cells. *Angewandte Chemie (International ed. in English)*, 56(30), 8801–8804. <https://doi.org/10.1002/anie.201702898>
  22. Wang, X. Q., Gao, F., & Zhang, X. Z. (2017). Initiator-loaded gold nanocages as a light-induced free-radical generator for cancer therapy. *Angewandte Chemie (International ed. in English)*, 56(31), 9029–9033. <https://doi.org/10.1002/anie.201703159>
  23. Hildebrandt, B., Wust, P., Ahlers, O., Dieing, A., Sreenivasa, G., Kerner, T., et al. (2002). The cellular and molecular basis of hyperthermia. *Critical Reviews in Oncology Hematology*, 43(1), 33–56. [https://doi.org/10.1016/S1040-8428\(01\)00179-2](https://doi.org/10.1016/S1040-8428(01)00179-2)
  24. Xie, X., Shao, X., Gao, F., Jin, H., Zhou, J., Du, L., et al. (2011). Effect of hyperthermia on invasion ability and TGF-beta1 expression of breast carcinoma MCF-7 cells. *Oncology Reports*, 25(6), 1573–1579. <https://doi.org/10.3892/or.2011.1240>
  25. Samali, A., Holmberg, C. I., Sistonen, L., & Orrenius, S. (1999). Thermotolerance and cell death are distinct cellular responses to stress: Dependence on heat shock proteins. *FEBS Letters*, 461(3), 306–310. [https://doi.org/10.1016/S0014-5793\(99\)01486-6](https://doi.org/10.1016/S0014-5793(99)01486-6)
  26. Zininga, T., Ramatsui, L., & Shonhai, A. (2018). Heat shock proteins as immunomodulators. *Molecules*. <https://doi.org/10.3390/molecules23112846>
  27. Das, U., Behera, S. S., Singh, S., Rizvi, S. I., & Singh, A. K. (2016). Progress in the development and applicability of potential medicinal plant extract-conjugated polymeric constructs for wound healing and tissue regeneration. *Phytotherapy Research*, 30(12), 1895–1904. <https://doi.org/10.1002/ptr.5700>
  28. Correia, M., Neves-Petersen, M. T., Parracino, A., di Gennaro, A. K., & Petersen, S. B. (2012). Photophysics, photochemistry and energetics of UV light induced disulphide bridge disruption in apo-alpha-lactalbumin. *Journal of Fluorescence*, 22(1), 323–337. <https://doi.org/10.1007/s10895-011-0963-7>
  29. Dietlin, C., Trinh, T. T., Schweizer, S., Graff, B., Morlet-Savary, F., Noirot, P. A., & Lalevee, J. (2020). New phosphine oxides as high performance near-UV type I photoinitiators of radical polymerization. *Molecules*. <https://doi.org/10.3390/molecules25071671>
  30. Beil, A., Steudel, F. A., Brauchle, C., Grutzmacher, H., & Mockl, L. (2019). Bisacylphosphane oxides as photo-latent cytotoxic agents and potential photo-latent anticancer drugs. *Science and Reports*, 9(1), 6003. <https://doi.org/10.1038/s41598-019-42026-y>
  31. Sorbellini, E., Rucco, M., & Rinaldi, F. (2018). Photodynamic and photobiological effects of light-emitting diode (LED) therapy in dermatological disease: An update. *Lasers in Medical Science*, 33(7), 1431–1439. <https://doi.org/10.1007/s10103-018-2584-8>
  32. Jandt, K. D., & Mills, R. W. (2013). A brief history of LED photopolymerization. *Dental Materials*, 29(6), 605–617. <https://doi.org/10.1016/j.dental.2013.02.003>
  33. Liu, J. H., Chen, Y. G., Yu, B. Y., & Chen, Y. J. (2006). A novel ketone derivative of artemisinin biotransformed by *Streptomyces griseus* ATCC 13273. *Bioorganic and Medicinal Chemistry Letters*, 16(7), 1909–1912. <https://doi.org/10.1016/j.bmcl.2005.12.076>
  34. Zeng, B., Cai, Z., Lalevee, J., Yang, Q., Lai, H., Xiao, P., et al. (2021). Cytotoxic and cytocompatible comparison among seven photoinitiators-triggered polymers in different tissue cells. *Toxicology in Vitro*, 72, 105103. <https://doi.org/10.1016/j.tiv.2021.105103>
  35. Zhang, J., Xiao, P., Morlet-Savary, F., Graff, B., Fouassier, J. P., & Lalevee, J. (2014). A known photoinitiator for a novel technology: 2-(4-methoxystyryl)-4,6-bis(trichloromethyl)-1,3,5-triazine for near UV or visible LED. *Polymer Chemistry*, 5(20), 6019–6026. <https://doi.org/10.1039/C4PY00770K>
  36. Ozben, T. (2007). Oxidative stress and apoptosis: Impact on cancer therapy. *Journal of Pharmaceutical Sciences*, 96(9), 2181–2196. <https://doi.org/10.1002/jps.20874>
  37. Tang, R. X., Kong, F. Y., Fan, B. F., Liu, X. M., You, H. J., Zhang, P., & Zheng, K. Y. (2012). HBx activates FasL and mediates HepG2 cell apoptosis through MLK3-MKK7-JNKs signal module. *World Journal of Gastroenterology*, 18(13), 1485–1495. <https://doi.org/10.3748/wjg.v18.i13.1485>
  38. Wang, H., Zhang, T., Sun, W., Wang, Z., Zuo, D., Zhou, Z., et al. (2016). Erianin induces G2/M-phase arrest, apoptosis, and autophagy via the ROS/JNK signaling pathway in human osteosarcoma cells in vitro and in vivo. *Cell Death and Disease*, 7(6), e2247. <https://doi.org/10.1038/cddis.2016.138>
  39. Wu, Q., Wu, W., Fu, B., Shi, L., Wang, X., & Kuca, K. (2019). JNK signaling in cancer cell survival. *Medicinal Research Reviews*, 39(6), 2082–2104. <https://doi.org/10.1002/med.21574>
  40. Park, J. G., Aziz, N., & Cho, J. Y. (2019). MKK7, the essential regulator of JNK signaling involved in cancer cell survival: A newly emerging anticancer therapeutic target. *Therapeutic Advances in Medical Oncology*, 11, 1758835919875574. <https://doi.org/10.1177/1758835919875574>
  41. Tar, H., Sevinc Esen, D., Aydin, M., Ley, C., Arsu, N., & Allonas, X. (2013). Panchromatic type II photoinitiator for free radical polymerization based on thioxanthone derivative. *Macromolecules*, 46(9), 3266–3272. <https://doi.org/10.1021/ma302641d>
  42. Lima, A. F., Salvador, M. V. O., Dressano, D., Saraceni, C. H. C., Gonçalves, L. S., Hadis, M., & Palin, W. M. (2019). Increased rates of photopolymerisation by ternary type II photoinitiator systems in dental resins. *Journal of the Mechanical Behavior of Biomedical Materials*, 98, 71–78. <https://doi.org/10.1016/j.jmbmm.2019.06.005>